

CORONAL TOMOGRAPHY

CHARLES C. KANKELBORG

Department of Physics, Montana State University, Bozeman, MT 59717

Draft version May 29, 2019

ABSTRACT

A simple, yet powerful, algorithm for computed tomography of the solar corona is demonstrated using synthetic EUV data. A minimum of three perspectives are required. These may be obtained from *STEREO*/EUVI plus an instrument near Earth, e.g. *TRACE* or *SOHO*/EIT.

Subject headings: methods: data analysis — Sun: corona — techniques: image processing

1. INTRODUCTION

Observations by the Extreme Ultraviolet Imager (EUVI, Wuelser et al. 2004) aboard *STEREO* provide the first simultaneous, stereoscopic image pairs of the solar corona and transition region. However, the 3D distribution of emission in the optically thin coronal volume remains difficult to estimate. The problem may be described as follows. Consider an object $I(x, y, z)$ on domain D . The coordinates x and y need not be orthogonal, but z is orthogonal to x and y . Given two projections $f(x, z) = \int_D I dy$ and $g(y, z) = \int_D I dx$, a plausible reconstruction of I is

$$I'(x, y, z) = \frac{f(x, z) g(y, z)}{T(z)}, \quad (1)$$

where $T(z) = \int_D I(x, y) dx dy = \int_D f(x) dx = \int_D g(y) dy$ is the total emission of a plane of constant z . Unfortunately, this solution fails utterly in practice. For each pair of sources in I , I' introduces a pair of “ghost” artifacts. These are systematic errors, independent of the noise and apparently unavoidable. Traditional regularization strategies are not fruitful: I' is positive, is as smooth as the observed images f and g , and is precisely the maximum entropy solution. More information is therefore required to guide the tomographic reconstruction.

Previously described approaches to the *STEREO* coronal tomography problem rely on assumptions about the geometry of the coronal plasma distribution. The triangulation method (Aschwanden 2005) assumes loops with circular cross-section, and relies on the identification of the same loops in both images. The magnetic tomography approach (Wiegelmann & Inhester 2006) also assumes loops with circular cross-section, and incorporates magnetic field extrapolations to constrain loop geometries. These methods are promising, but in both cases the 3D reconstruction requires assumptions about things that one might reasonably hope to learn from the 3D reconstruction.

I propose that EUV images taken from a third perspective — e.g. *TRACE* or *SOHO*/EIT — may provide adequate additional constraints for coronal tomography, without any assumptions about loop geometry or magnetic fields. I describe a simple computed tomography algorithm, fast enough to run in real time, and demonstrate its performance using synthetic data with three viewpoints.

2. ALGORITHM

The Smooth Multiplicative Algebraic Reconstruction Technique (SMART) presented here has been devel-

oped to solve a mathematically analogous problem of reconstructing spectra for the *MOSES* sounding rocket payload (Kankelborg & Thomas 2001; Fox et al. 2003). SMART is related to multiplicative algebraic reconstruction techniques that have been available for many years (Okamoto & Yamaguchi 1991; Verhoeven 1993). The unique features of SMART are iterative smoothing and an adaptive correction strategy. These refinements improve numerical stability and promote convergence to a compromise between smoothness and goodness-of-fit, leading to a reduced chi-squared of unity.

In the N -view tomography problem, an object $I(x, y, z)$ on domain D is known only by N projections f_m , taken at angles θ_m :

$$f_m(x, z) = \int_D \mathcal{R}(\theta_m) I(x, y, z) dy. \quad (2)$$

The operator $\mathcal{R}(\theta_m)$ rotates the object I by angle θ_m about the z axis.¹ SMART uses the projections f_m to estimate $I(x, y, z)$ as follows.

1. Create an initial guess, $I'(x, y, z) = 1$ on D .
2. Initialize correction weights, $\gamma_m = \frac{1}{N}$.
3. Apply smoothing, $I' \leftarrow I' * K$.
4. Calculate projections $f'_m(x, z) = \int_D \mathcal{R}(\theta_m) I' dy$.
5. Calculate correction factors,

$$C_m(x, y, z) = \mathcal{R}(-\theta_m) \frac{f'_m(x, z)}{f_m(x, z)}. \quad (3)$$

Note that a nontrivial y -dependence is introduced through the rotation.

6. Apply corrections weighted by γ_m ,

$$I' \leftarrow I' \prod_m C_m^{\gamma_m}. \quad (4)$$

7. Calculate reduced chi-squared for each projection, $\chi_{R,m}^2$.
8. Adjust correction weights, γ_m , using a control law designed to drive $\chi_{R,m}^2 \rightarrow 1$.

¹ Rotation \mathcal{R} could incorporate compound angles with altitude, azimuth and roll. The extension of SMART to the most general case is trivial.

9. Repeat steps 3-8 until converged.

The subphotospheric portion of the I' array is zeroed in step 1, and will remain zero since the corrections are multiplicative (eq. [4]).

Since the correction factors (eq. [3]) are ratios of positive numbers, the reconstruction is always positive. The strength of the m th applied correction is governed by γ_m . Step 8 sets up feedback to establish a dynamic equilibrium between smoothing and correction, so that χ_{Rm}^2 tends toward unity. Our control law, which has two adjustable parameters (a, b), modifies γ_m using a linear combination of the previous and current values of χ_{Rm}^2 :

$$\Delta\gamma_m = aX_m + b\Delta X_m, \quad X_m \equiv \log(\chi_{Rm}^2) \quad (5)$$

The algorithm is implemented in IDL, with rotations $\mathcal{R}(\theta_m)$ performed via cubic convolutional interpolation. It is possible that spurious negative voxels could be introduced during the rotation associated with projection, but negative values are eliminated from our projections by thresholding: $f_m \geq 0$.

The normalized smoothing kernel, $K(x, y, z)$, is defined on the discrete space of voxels as follows:

$$K_{ijk} = \frac{\delta_{ijk} + s c^{(i+j+k)}}{1 + s(1 + 4c + 12c^2 + 8c^3)}, \quad c \equiv \frac{2}{5}. \quad (6)$$

This form of K is not crucial, but it is designed to be very nearly isotropic. The adjustable smoothing parameter, $s \in (0, 1]$, affects the rate of convergence but has no discernible effect on the result.

3. SYNTHETIC DATA

A volume of synthetic coronal emissivities was prepared as a test target for the SMART algorithm. I began with a potential field defined by four sub-photospheric magnetic charges. The resulting line-of-sight photospheric magnetic field is shown in figure 1. As shown in the figure, five small “heated” patches were defined among the positive polarities on the photospheric plane. A large number of field lines were shot through the volume to define coronal features connected to these patches. The “true” columns in figures 2 and 4 show the volume model from a variety of perspectives. All images of EUV emission in this letter are square root scaled to bring out faint features. The coronal features have complicated geometries. A coronal magnetic null within the tallest coronal feature results a broad, vertical fan of emission above the positive pole.

Numerous synthetic observations of the model coronal volume were produced, each time choosing random tilt over the interval $[-180^\circ, 180^\circ]$, a random northern heliographic latitude over $[0^\circ, 30^\circ]$, and a random heliographic longitude over $[-50^\circ, 50^\circ]$. Observations were projected for three distant virtual instruments, observing along heliographic longitudes $-40^\circ, 0^\circ, 40^\circ$. The twin *STEREO* spacecraft will reach similar separation angles in October, 2008. The images were normalized so that the brightest pixel among the three images had 3000 counts. The $(-40^\circ, 0^\circ, 40^\circ)$ projections under the “true” columns in figures 2 and 3 correspond to two example observations. Poisson noise was applied to the images prior to passing them to the SMART algorithm for inversion. Square root scaled to show the photon noise more clearly. The mean value of the nonzero pixels is 216 counts. This example is used for the figures throughout this Letter.

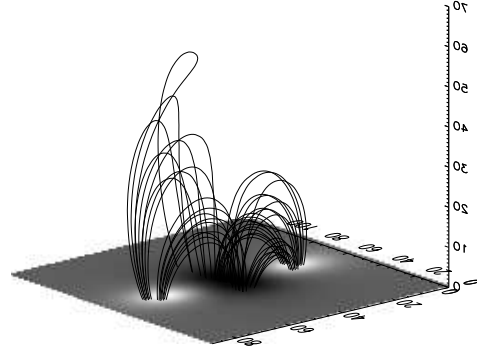


FIG. 1.— Vertical magnetic field (shaded plane) and field lines corresponding to the model corona. Note the sharp deflection of the uppermost field line from the coronal null.

4. INVERSION RESULTS

The synthetic data were inverted using a fixed number of 15 SMART iterations. This was typically sufficient to converge to $\chi_{Rm}^2 = 1 \pm 0.01$. The rate of convergence is affected by the smoothing parameter and by the two adjustable parameters in the control law. The example used $s = 0.5$, $a = 0.05$, $b = 0.16$. Within broad limits, the results are insensitive to these parameters. For example, if the smoothing is removed altogether, numerical instabilities arise; if it is made too strong, then it will not be possible to reach $\chi_{Rm}^2 = 1$. For our computational volume of 169^3 voxels, an inversion runs in a few minutes on a laptop computer.

Figure 2 compares noise-free visualizations of a coronal volume model to its tomographic reconstruction from seven viewpoints in the ecliptic plane. Figure 4 provides a similar comparison, moving up out of the ecliptic. All features have been recovered. Square root scaling helps to bring out the artifacts, which are few and faint. There is slight blurring, and minimal ghosting. These results are typical of the many realizations tried so far.

A second example, with loops nearly parallel to the ecliptic plane, is given in figures 3 and 5. This orientation is very difficult because only the ends of horizontal features provide any depth cues. Although the ecliptic views are reproduced well, the example shows poor reconstruction of the out-of-ecliptic views. Animated visualizations of figures 2-5 are provided in the electronic version of the Journal.

5. DISCUSSION AND CONCLUSIONS

Coronal tomography is possible with as few as three viewpoints, making no prior assumptions about coronal morphology or magnetic fields. The test cases demonstrate recovery of complex geometry that would be excluded by assumption in any of the previously published techniques. Our examples also illustrate that horizontal loops provide insufficient depth cues for an array of instruments confined to the ecliptic.

The *STEREO* mission will obtain data at large separation angles in Fall 2008. Observations from *SOHO* and/or *TRACE* at that time should allow the first application of SMART to coronal tomography.

ACKNOWLEDGMENTS

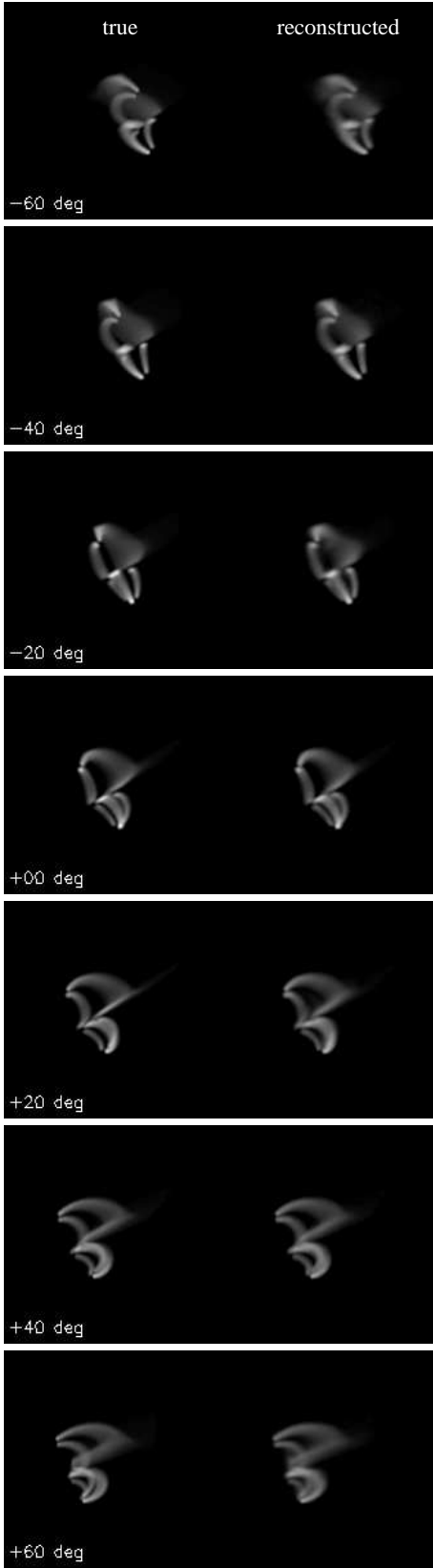


FIG. 2.— Comparison of true and reconstructed coronal volumes, panning in the ecliptic plane. Intensities are square root scaled.

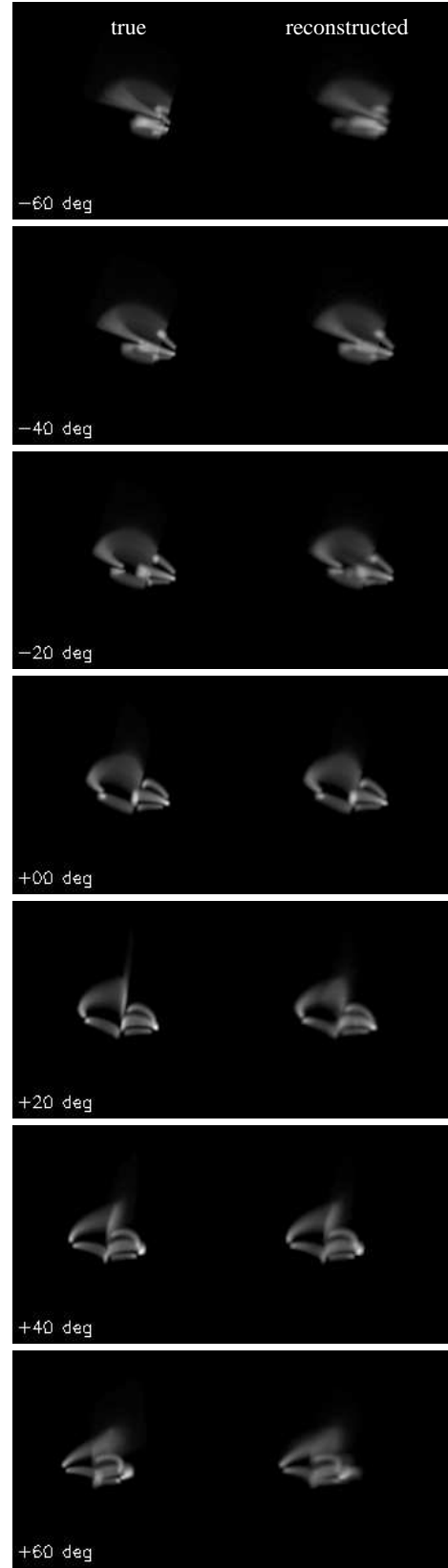


FIG. 3.— Same as figure 2, but with loops nearly parallel to the ecliptic.

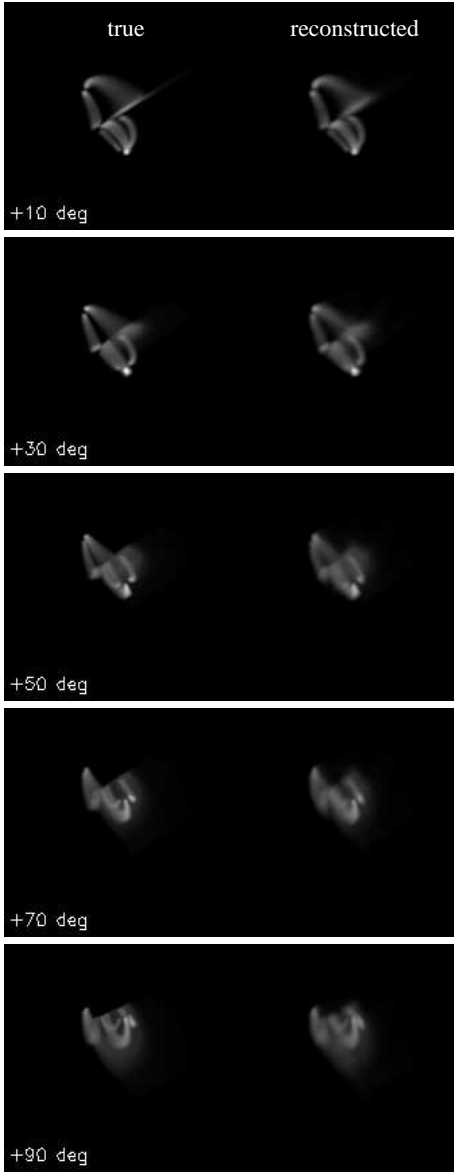


FIG. 4.— Comparison of true and reconstructed coronal volumes, moving up the central heliographic meridian at five different latitudes. Intensities are square root scaled.

I thank Dana Longcope for many helpful suggestions made during the preparation of this Letter. This work was supported by NASA grant NNX07AG6G.

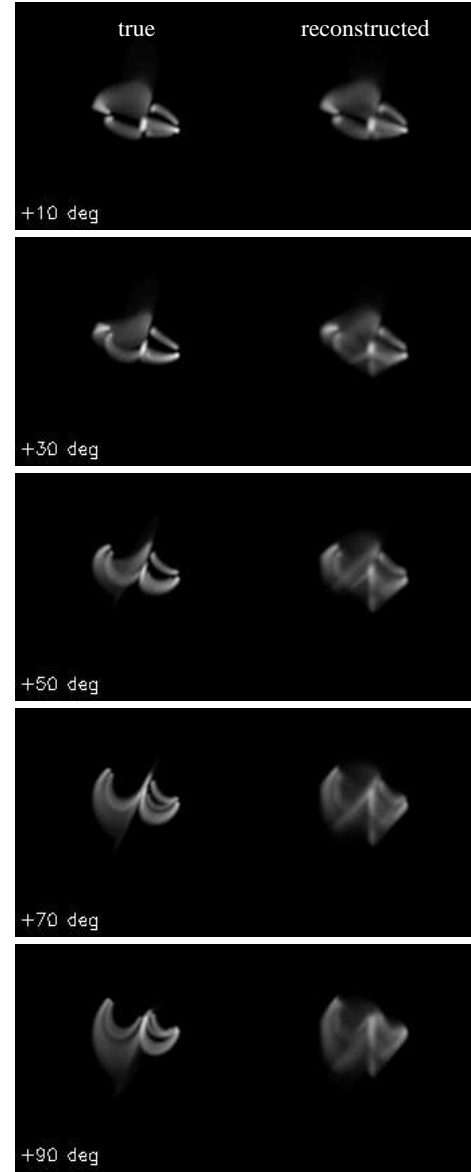


FIG. 5.— Same as figure 4, but with loops nearly parallel to the ecliptic.

REFERENCES

- Aschwanden, M. J. 2005, *Sol. Phys.*, 228, 339
- Fox, J. L., Kankelborg, C. C., & Metcalf, T. R. 2003, in *Optical Spectroscopic Techniques and Instrumentation for Atmospheric and Space Research V*, Larar, Allen M.; Shaw, Joseph A.; Sun, Zhaobo., eds. Proc. SPIE, Vol. 5157, 124–132
- Kankelborg, C. C. & Thomas, R. J. 2001, in *Visible Space Instrumentation for Astronomy and Solar Physics*, Oswald H. Siegmund; Silvano Fineschi; Mark A. Gummin; Eds., Proc. SPIE, Vol. 4498, 16–26
- Okamoto, T. & Yamaguchi, I. 1991, *Optics Letters*, 16, 1277
- Verhoeven, D. 1993, *Applied Optics*, 32, 3736
- Wiegmann, T. & Inhester, B. 2006, *Sol. Phys.*, 236, 25
- Wuelser, J.-P., Lemen, J. R., Tarbell, T. D., Wolfson, C. J., Cannon, J. C., Carpenter, B. A., Duncan, D. W., Gradwohl, G. S., Meyer, S. B., Moore, A. S., Navarro, R. L., Pearson, J. D., Rossi, G. R., Springer, L. A., Howard, R. A., Moses, J. D., Newmark, J. S., Delaboudiniere, J.-P., Artzner, G. E., Auchere, F., Bougnet, M., Bouyries, P., Bridou, F., Clotaire, J.-Y., Colas, G., Delmotte, F., Jerome, A., Lamare, M., Mercier, R., Mullot, M., Ravet, M.-F., Song, X., Bothmer, V., & Deutsch, W. 2004, in *Telescopes and Instrumentation for Solar Astrophysics*, Proc. SPIE, ed. S. Fineschi & M. A. Gummin, Vol. 5171, 111–122